J. Fluid Mech. (2021), *vol*. 906, A5. © The Author(s), 2020.
Published by Cambridge University Press
doi:10.1017/jfm.2020.791

The impact of an oil droplet on an oil layer on water

Dohyung Kim[1], Jinseok Lee[1], Arijit Bose[2], Ildoo Kim[3],† and Jinkee Lee[1],†

[1]School of Mechanical Engineering, Sungkyunkwan University, Suwon, Gyeonggi-do 16419, Republic of Korea

[2]Department of Chemical Engineering, University of Rhode Island, Kingston, RI 02881, USA

[3]Department of Mechatronics, Konkuk University, Chungju 27478, Republic of Korea

(Received 17 March 2020; revised 6 September 2020; accepted 14 September 2020)

We present a study of droplet impingement on a two-layer liquid, specifically an oil droplet impinging on a layer of oil on water. In our experiments, the diameter and impact velocity of the droplet and the thickness of the oil layer were varied, and the maximum depth of the crater and the maximum height of the Worthington jet were measured. When the thickness of the oil layer was less than ∼1.6 times the droplet diameter, the depth of the crater depended on the thickness of the oil layer. Otherwise, the two-layer liquid behaved like a single layer. This observation is rationalized by considering the oil–water interface, whose deformation is negligible when the oil layer is thick but becomes significant when the oil layer is thinner. We define an effective Weber number for the two-layer liquid and show that the height of the Worthington jet is proportional to this effective Weber number.

Key words: interfacial flows (free surface)

1. Introduction

The impingement of a liquid droplet on another liquid has been studied extensively (Pumphrey & Elmore 1990; Wang & Chen 2000; Cossali *et al.* 2004; Bisighini *et al.* 2010; Castillo-Orozco *et al.* 2015; Che & Matar 2018; Shaikh *et al.* 2018). When a droplet impinges on a deep pool of the same liquid, e.g. a water droplet on a water bath (Engel 1965), a crater and a crown-like structure are created in the target liquid. When a liquid droplet falls onto a solid surface, no crater can be created, and only a crown-like structure is formed (Che & Matar 2018; Shaikh *et al.* 2018). In addition, various systems with differing miscibilities between the droplet and the target liquid have been investigated, such as water droplet–water pool and oil droplet–water pool systems (Jain *et al.* 2019) and a water droplet–oil pool (Fujimatsu *et al.* 2003; Xu, Wang & Lu 2017). A more complex situation arises when a droplet impinges on a two-layer liquid. For example, Murphy *et al.* (2015) studied a water drop impacting on oil-covered seawater and observed that the oil layer ruptures on impact. Another study (Wang *et al.* 2019) found that such an impact produces oil–water emulsions.

† Email addresses for correspondence: ildoo.kim.phys@gmail.com, lee.jinkee@skku.edu

In this study, we focused on the impingement of an oil droplet on a two-layered liquid: an oil layer on a deep pool of water. Such a configuration is important when considering the emulsification of oil following a spill in fresh water or seawater. To treat such spills, dispersant-containing droplets are typically released from a low-flying aircraft onto the oil layer on the water's surface (Lessard & DeMarco 2000; Fingas 2012). When a droplet impinges on a deep pool of liquid, the depth of the crater d is proportional to the fourth root of the Froude number $Fr \equiv U^2/gD$, where U is the impact velocity, g is the acceleration due to gravity and D is the droplet diameter (Pumphrey & Elmore 1990; Leng 2001; Fedorchenko & Wang 2004; Ray, Biswas & Sharma 2015). However, such a scaling relation is not necessarily valid when an oil layer exists on top of the water.

To define the scaling relationship in the presence of an oil layer, we constructed a typical experimental set-up for studying the impingement of a droplet on a liquid bath. We carefully deposited a layer of hexadecane on water, and a hexadecane droplet was then allowed to fall on the layer. We varied the diameter and impact velocity of the droplet and the thickness of the oil layer. We measured the depth of the crater as a function of Fr and the dimensionless thickness of the oil layer. As the crater closes, a Worthington jet (Worthington 1908) is ejected, and the height of this jet ℓ was also monitored.

We found that the scaling relation between the depth of the crater and Fr depended on the thickness of the oil layer. When the oil layer was thick, the measurements followed the classical model (Pumphrey & Elmore 1990), that is

$$d \sim Fr^{1/4} D. \tag{1.1}$$

Therefore, we can interpret that, when the layer is sufficiently thick, it can be approximately considered as demonstrating an infinite thickness.

However, when the oil layer was thin, our measurements deviated from the classical model. This is because the 'second' (oil–water) interface will play a role in such a situation. For quantitative characterization, we established a dual-interface model. Our model was based on the work of Engel (1965), but it was modified to take into account the presence of the second interface between the oil layer and the underlying water in addition to the first one between the air and the oil layer. When a droplet impinges on the target liquid and creates a crater, the gravitational potential energy of the fluid displaced by the impact depends on the density of the fluid. Therefore, it is correctly estimated only when both the oil and the water are considered. The model allows us to calculate the change in the surface energy due to the deformation of the second interface. The combination of these two effects yielded the correct scaling relationship for our measurements.

Using the dual-interface model, we can estimate the height of the jet and the vertical position at which the pinch-off of a child droplet will occur. First, we define an effective surface tension σ_e and an effective Weber number We_e such that $We_e = \rho_o U^2 D/\sigma_e$, where ρ_o is the density of the oil. The height of the jet increases with We_e or, equivalently, the oil layer thickness. The pinch-off position is determined by the ejection speed of the jet, which is correlated with the jet height (Ghabache, Séon & Antkowiak 2014; Kim, Kim & Jung 2018). The dual-interface model therefore allows us to classify the pinch-off modes.

The following sections describe our experimental set-up and conditions (§ 2), the overview of the sequential images showing the impact process (§ 3), the details of craters (§ 3.1), a dual-interface model to explain our results (§ 3.2) and the details of jets (§ 3.3). Finally, we summarize and conclude the whole results (§ 4).

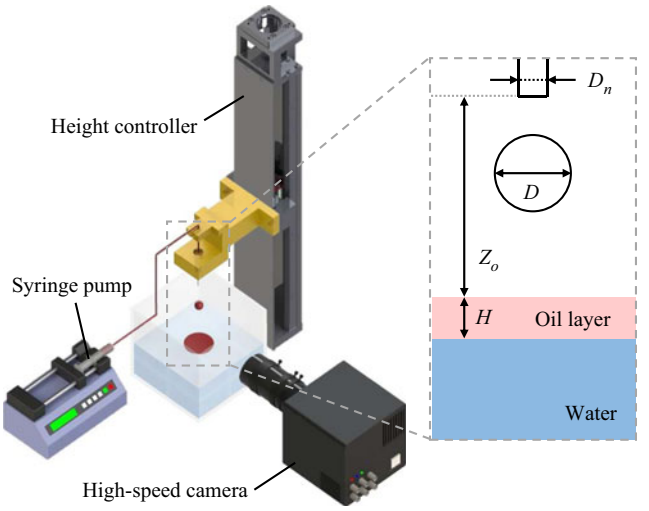

FIGURE 1. A schematic diagram of the experimental set-up. Oil droplets are prepared by pushing oil through a needle using the syringe pump. Each droplet falls onto an oil layer on water, and the event is recorded by a high-speed camera. The impact velocity is varied by changing the height of the needle using a translational stage.

2. Experimental set-up

Our experiments were carried out using the apparatus shown in figure 1. The set-up is similar to those used in other experimental studies (Castillo-Orozco *et al.* 2015; Che & Matar 2018; Jain *et al.* 2019). The equipment comprises two parts: a droplet dispenser and an acrylic bath. An oil droplet prepared by the dispenser falls onto the target liquid in the acrylic bath (Smolka & McLaughlin 2019). The impact between the droplet and the target liquid produces a splash, which is recorded by high-speed video imaging. For the oil component, we used hexadecane, which exhibits the following properties: density $\rho_o = 770\ \mathrm{kg\ m^{-3}}$, interfacial tension with air $\sigma_{oa} = 27.2\ \mathrm{mN\ m^{-1}}$, interfacial tension with water $\sigma_{ow} = 55.2\ \mathrm{mN\ m^{-1}}$ and kinematic viscosity $\nu_o = 3.95 \times 10^{-6}\ \mathrm{m^2\ s^{-1}}$ at room temperature (Goebel & Lunkenheimer 1999).

An oil droplet is produced by pushing the oil through a needle using a syringe pump. The syringe pump is connected to the needle and pushes oil at $1.67\ \mu\mathrm{l\ s^{-1}}$. At the tip of the needle, a pendent droplet grows in time and is released when the gravitational force becomes greater than the surface tension force, i.e. $\rho_o V g = \pi \sigma_{oa} D_n$, where V is the volume of the droplet and D_n is the diameter of the needle. Therefore, the diameter of the falling droplet D is obtained using

$$D = \left(\frac{6\sigma_{oa} D_n}{\rho_o g} \right)^{1/3}. \tag{2.1}$$

In this study, we used three different needles with $D_n = 0.380$, 0.750 and 1.60 mm to produce droplets of $D = 2.02$, 2.53 and 3.26 mm, respectively.

The impact velocity was varied by changing the height of the needle z_0. For $z_0 = 50$, 250, 450 and 750 mm, we established velocities of $U \simeq 1.0$, 2.2, 2.8 and $3.5\ \mathrm{m\ s^{-1}}$, respectively. The calculation of U was based on a mathematical model in which only the gravitational force and the form drag are considered (Pumphrey & Elmore 1990), that

Case	D (mm)	z_0 (mm)	U (m s^{-1})	*We*	*Re*	$H' \equiv H/D$	$\overline{H'}$
A1	2.02	50	0.98	54.9	503	0, 0.39, 1.10	
A2		250	2.14	259	1090	0, 0.56, 0.86, 2.58	
A3		450	2.79	441	1430	0, 0.34, 0.96, 2.86	
A4		750	3.45	678	1770	0, 0.50, 0.90, 2.65	
B1	2.53	50	0.98	69.0	632	0, 0.43, 0.85	
B2		250	2.15	330	1380	0, 0.38, 0.77, 2.05	0, 0.38, 0.81, 2.21
B3		450	2.82	568	1810	0, 0.33, 0.77, 2.28	
B4		750	3.53	886	2090	0, 0.39, 0.79, 2.11	
C1	3.26	50	0.99	89.3	750	0, 0.37, 0.86	
C2		250	2.17	431	1650	0, 0.33, 0.77, 1.60	
C3		450	2.86	474	2270	0, 0.29, 0.65, 1.77	
C4		750	3.59	1180	2970	0, 0.31, 0.58, 1.64	

TABLE 1. Experimental conditions. We tested 12 cases, composed of three different values of D and four different values of U. In each case, the droplet impacted four different thicknesses of oil layer. The thicknesses of the oil layers are shown. We categorized the thickness of oil layers by taking an average of all cases such that $\overline{H'} = 0$ (no oil layers), 0.38 (thinner oil layers), 0.81 (thin oil layers) and 2.21 (thick oil layers).

is,

$$U = U_t \left[1 - \exp\left(-\frac{2g}{U_t^2} z_0\right)\right]^{1/2}, \tag{2.2}$$

where the terminal velocity $U_t = (4\rho_o Dg/3\rho_a C_d)^{1/2}$, in which ρ_a is the density of air and C_d is the drag coefficient of a sphere. We also made the measurement of U by analysing video frames recorded by a high-speed camera, whose set-up is discussed later. The measurement matched the calculation using (2.2) within 4 %, and this agreement also confirms that the estimation of D using (2.1) is correct.

The tank was filled with water, and hexadecane was gently deposited on the surface using a syringe. We note that the tank was thoroughly cleaned before each run to ensure that all surfaces are free of contamination. As the oil is deposited, it spreads to form a thin layer of thickness H. We used four different thicknesses of oil layer: (i) no oil layer ($\bar{H} = 0$), (ii) a thinner oil layer ($\bar{H} = 0.98$ mm), (iii) a thin oil layer ($\bar{H} = 2.16$ mm) and (iv) a thick oil layer ($\bar{H} = 5.51$ mm), where the bar on H indicates that averages of various runs were taken. However, we defined and used the non-dimensional thickness of the oil layer $H' = H/D$, and $\overline{H'}$ as the average of H' for all tested cases, because this is more relevant for physical description and analysis. The parameter $\overline{H'}$ is used to describe and compare the impingement results depending on the thickness of the oil layer in §§ 3.1–3.3. For thinner oil layers $\overline{H'} = 0.38$, for thin oil layers $\overline{H'} = 0.81$, and for thick oil layers $\overline{H'} = 2.21$. A full list of the experimental conditions is summarized in table 1. We also note that the size of the tank is large enough (150 mm × 150 mm × 150 mm) that the reflection of capillary waves by the walls of the tank is negligible (Yilmaz & Nelson 2014).

We recorded shadowgraphic images using a high-speed camera (FASTCAM Mini UX100, Photron) with a zoom lens (MLH-10X, Computar). The droplet was illuminated by a light-emitting diode lamp (E4-1.2BF, Alpha Lite Co. Ltd) installed on the opposite side of the tank to the camera. The images were captured at 10 000 frames per second. The video frames were then processed by using software written in-house using MATLAB

(MathWorks), from which we directly measured the length scales relevant to the droplet impact, such as the depth of the crater and the height of the Worthington jet.

Henceforth, we will use the primed variables to denote non-dimensional quantities, i.e. $H' = H/D$, $d' = d/D$ and $\ell' = \ell/D$.

3. Results and discussion

In figure 2, we present four sets of sequential images showing the impact process. Specifically, these sets show the impingement of an oil droplet of $D = 3.26$ mm on the underlying oil layers at an impact velocity $U = 2.17$ m s^{-1} (case C2 in table 1). The non-dimensional thicknesses of the oil layer H' were 0, 0.33, 0.77 and 1.60.

The impact process presented in figure 2 is, in general, similar to the classical impingement between a water droplet and a water bath (Prosperetti & Oguz 1993; Leng 2001; Manzello & Yang 2002; Michon, Josserand & Séon 2017). As the droplet pushes the target liquid, a crater is formed below the original level of the target liquid, and a crown-like structure rises above the rim of the crater (Macklin & Metaxas 1976). Shortly after the impact, the crater closes, and a Worthington jet is ejected from the point of impact. These features, both the formation of the crater and the ejection of the Worthington jet, are very typical (Ghabache *et al.* 2014; Michon *et al.* 2017) for the impact of a drop of liquid with the surface of another liquid.

Despite overall similarities, we found that the physical process of the impact was affected by the thickness of the oil layer in a non-monotonic manner. For example, both the depth of the crater d and the height of the jet ℓ are greater when $H' = 0$ and $H' = 1.60$ (figure 2*a*,*d*) than when $H' = 0.33$ or $H' = 0.77$ (figure 2*b*,*c*). This is intriguing, because we speculate that the oil layer acts to attenuate the kinetic energy of the impact, and a thicker oil layer produces a shallower crater. However, this expectation is not borne out by observations. Another example is the pinch-off time of child droplets, which is significantly delayed when the thickness of the oil layer is neither small nor large. In figure 2, it can be seen that the pinch-off occurs at 80 ms when $H' = 0.77$ but at 50 ms when $H' = 0$ or $H' = 1.60$. These non-monotonic dependences are also observed in other cases, for example case C4 in table 1 (see figure 3). These observations indicate that the oil layer cannot be approximated as a simple attenuator of the kinetic energy of an impinging droplet. As noted, we developed a dual-interface model, where the finite thickness of the oil layer is considered. This model was compared with the quantitative measurements from experiments.

3.1. *The depth of the crater*

In figure 4(*a*), we present the maximum depth of the crater $d' = d/D$ as a function of the Froude number $Fr = U^2/gD$ for four different thicknesses of oil layer. Each data point in the figure represents the average of three repeated measurements, and the error bars show the spreads of the measurements. It is noticeable in figure 4(*a*) that the relationship between d' and Fr depends on the thickness of the oil layer. For a thick oil layer, the measurement shows that d' follows the scaling relation in (1.1), $d' \sim Fr^{1/4}$, which is observed for the impingement of a liquid droplet onto the same liquid of large depth (Pumphrey & Elmore 1990). Physically, (1.1) is justified by the energetic analysis where the kinetic energy of the incoming droplet is transferred only to gravitational potential energy. Our data indicate that, when the oil layer is thick enough, it can be effectively approximated as a deep pool. In this condition, the underlying water bath does not

https://doi.org/10.1017/jfm.2020.791 Published online by Cambridge University Press

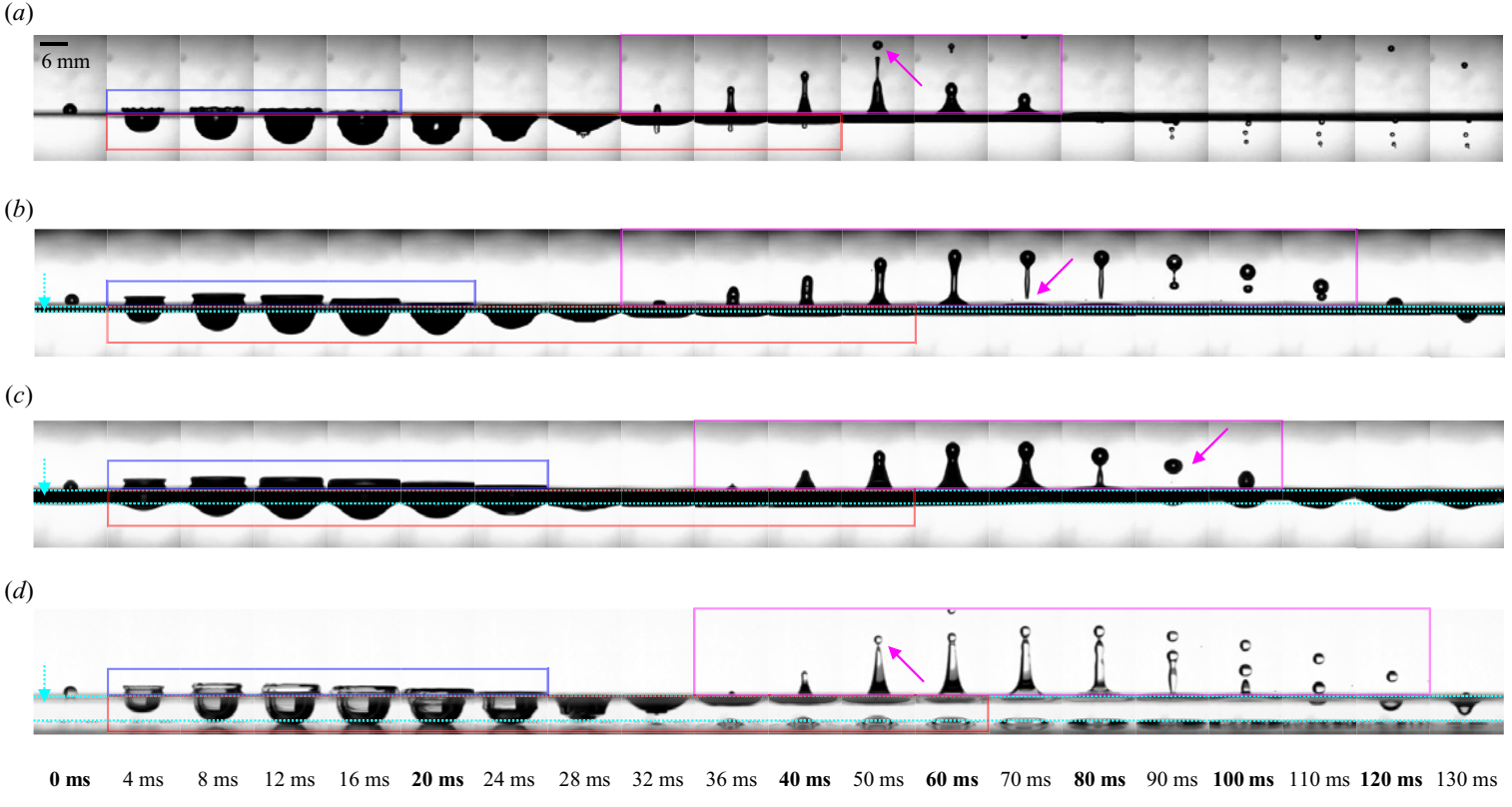

FIGURE 2. The impact process of the case C2 ($D = 3.26$ mm and $U = 2.17$ m s^{-1}). The non-dimensional thicknesses $H' \equiv H/D$ were: (*a*) $H' = 0$, no oil layer; (*b*) $H' = 0.33$, thinner oil layer; (*c*) $H' = 0.77$, thin oil layer; and (*d*) $H' = 1.60$, thick oil layer. The coloured boxes indicate the crater (red), crown-like structure (blue) and Worthington jet (magenta), and the arrows indicate the oil layer (cyan) and child droplets (magenta).

https://doi.org/10.1017/jfm.2020.791 Published online by Cambridge University Press

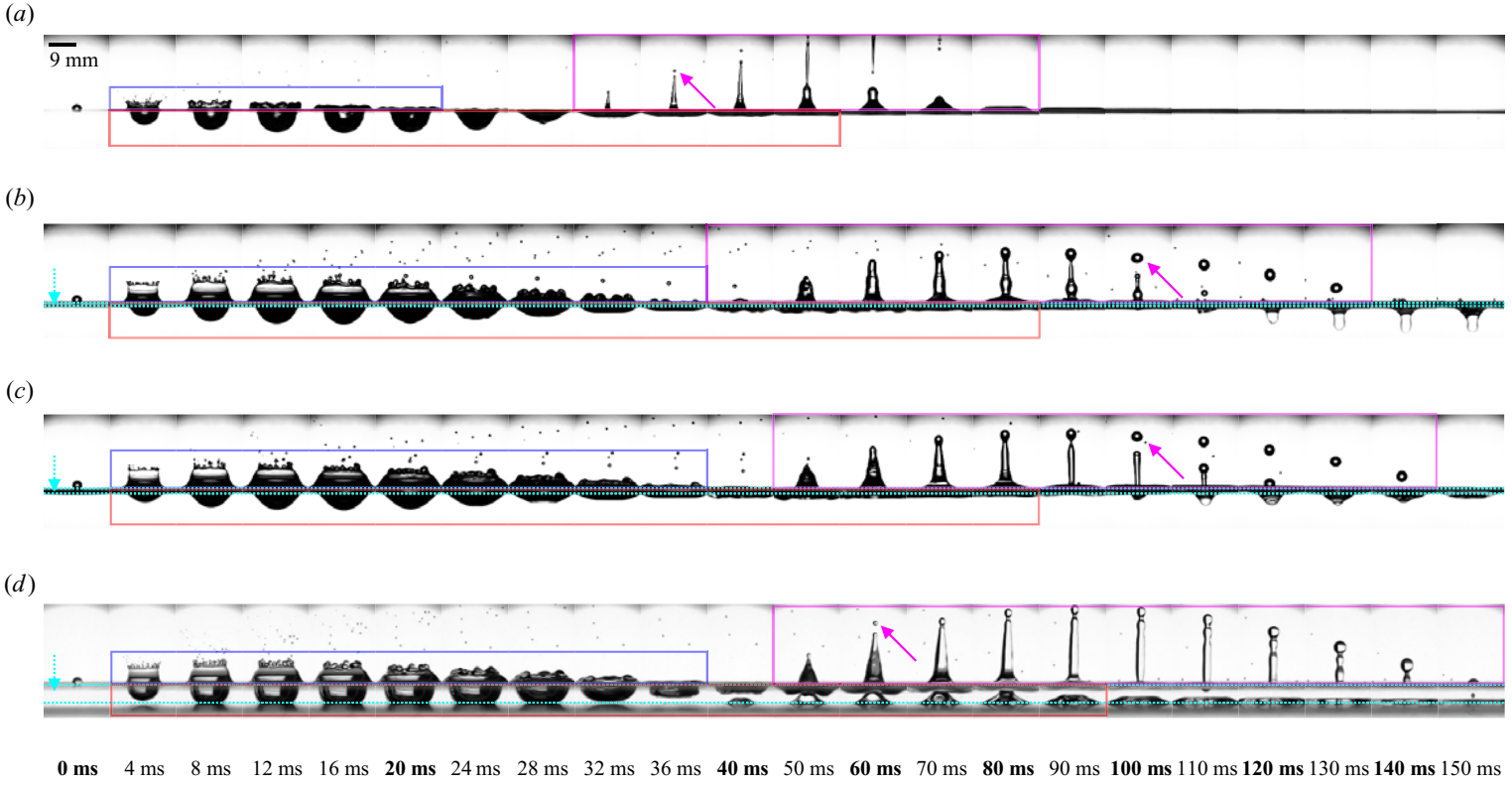

FIGURE 3. The impact process of the case C4 ($D = 3.26$ mm and $U = 3.59$ m s^{-1}). The non-dimensional thicknesses $H' \equiv H/D$ were: (*a*) $H' = 0$, no oil layer; (*b*) $H' = 0.31$, thinner oil layer; (*c*) $H' = 0.58$, thin oil layer; and (*d*) $H' = 1.64$, thick oil layer. The coloured boxes indicate the crater (red), crown-like structure (blue) and Worthington jet (magenta), and the arrows indicate the oil layer (cyan) and child droplets (magenta).

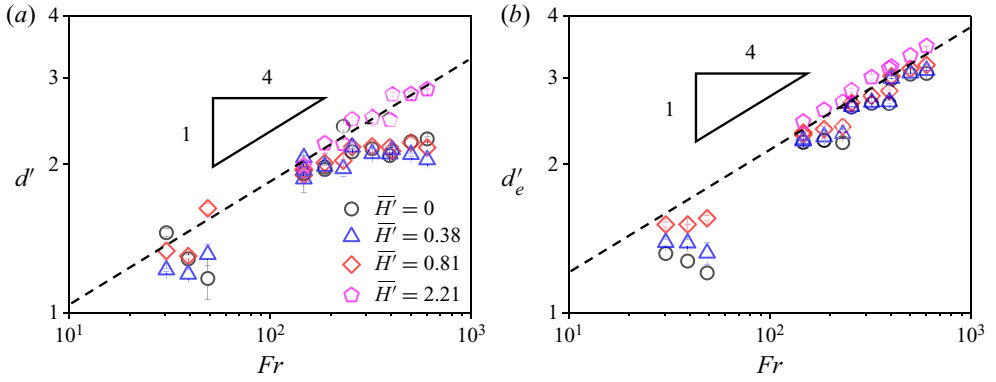

FIGURE 4. The dimensionless maximum depth of the crater, d', with respect to the Froude number $Fr \equiv U^2/gD$. (*a*) The measurement of d' for $\overline{H'} = 0$, 0.38, 0.81 and 2.21. (*b*) The calculated roots of (3.7), where d'_e, is the dimensionless maximum depth of the crater considering the extra surface energy of the second interface. The dashed lines were drawn to clarify the slope of 1/4.

influence the impact process, and we assume that $H' > 1.60$ is not distinguishable from the case where $H' \to \infty$, considering that $H' = 1.60$ for case C2.

However, for the thin or thinner oil layers, the scaling relation in (1.1) is no longer valid. Instead, d' is much shallower than in the case of the thick oil layer, as shown in figure 4(*a*). In these cases, a simple energy balance between the kinetic energy of the droplet and the gravitational potential energy of the crater is not valid. Instead, the kinetic energy of the incoming droplet is effectively reduced by the presence of the oil layer, and this effective reduction is more (less) substantial at larger (smaller) scales. This observation indicates that the surface energy from the deformation of the interface is not the sole source of the attenuation, and the gravitational potential energy of the two fluids must be considered individually.

The scaling relation also fails when there is no oil layer. In this case, considering the miscibility between the impinging droplet and the target liquid is necessary, and a spreading coefficient $S = \sigma_{ta} - \sigma_{td} - \sigma_{da}$, where the subscripts d, a and t represent the droplet, air and target liquid, respectively. In detail, when no oil layer ($H' = 0$) exists, the impinging droplet and the target liquid are immiscible, unlike in a classical miscible drop impact. Jain *et al.* (2019) shows that the scaling relation in (1.1) is also valid when a silicone oil droplet impinges onto water, even though the impinging droplet and the target liquid are immiscible. However, we used hexadecane oil as the impinging droplet, which exhibits a negative spreading coefficient on water ($S = \sigma_{wa} - \sigma_{wo} - \sigma_{oa} \simeq -10$ mN m$^{-1} < 0$, where $\sigma_{wa} = 72$ mN m^{-1}). This is in contrast to silicone oil, which exhibits a positive spreading coefficient on water ($S \simeq 15$ mN m$^{-1} > 0$) (Goebel & Lunkenheimer 1999; Boreyko *et al.* 2014).

3.2. *The dual-interface model*

To quantitatively account for the presence of the oil layer, we present a simple geometric model, as shown in figure 5, where the target liquid consists of two immiscible fluids. We assume that, as an oil droplet of size D impinges on the target liquid, a hemispherical crater

of radius d is formed. Before the collision, the kinetic energy of the incoming droplet is

$$E_k = \frac{\pi}{12}\rho_o D^3 U^2. \tag{3.1}$$

After the collision, the gravitational potential energy of the displaced fluid is expressed as

$$E_p = -(\rho_t V_c) g d_c, \tag{3.2}$$

where ρ_t is the density of the target liquid, V_c is the volume of the crater and d_c is the centroid of the crater. The minus sign indicates that the displacement of the target liquid subtracts E_p from the system. We then use $V_c = \int_{z_1}^{z_2} \pi(d^2 - z^2)\ \mathrm{d}z$ and $d_c = (1/V_c)\int_{z_1}^{z_2} \pi(d^2 - z^2)z\ \mathrm{d}z$, where z_1 and z_2 denote the vertical range of the integral. When no oil layer ($H = 0$) or a thick oil layer ($H > d$) exists, the range of the integral is simply $[-d, 0]$ to cover the whole of the hemispherical crater, and we obtain $V_c = (2/3)\pi d^3$ and $d_c = -(3/8)d$. Therefore,

$$E_p = \begin{cases} \dfrac{\pi}{4}\rho_w g d^4 & \text{for } H = 0, \\ \dfrac{\pi}{4}\rho_o g d^4 & \text{for } H > d, \end{cases} \tag{3.3}$$

where ρ_w is the density of water. When the thickness of the oil layer is neither zero nor thick enough, i.e. $0 < H < d$, the integral is divided into two ranges to cover the oil part and the water part. Therefore,

$$\begin{aligned} E_p &= -\rho_o g \int_{-H}^{0} \pi(d^2 - z^2)z\ \mathrm{d}z - \rho_w g \int_{-d}^{-H} \pi(d^2 - z^2)z\ \mathrm{d}z \\ &= \frac{\pi}{4}\rho_o g d^4 + \frac{\pi}{4}(\rho_w - \rho_o) g (d^2 - H^2)^2. \end{aligned} \tag{3.4}$$

We note that (3.4) converges to (3.3) as $H \to 0$ or $H \to d$.

Next, we consider the change in the surface energy before and after the impingement. As shown in figure 5, the target liquid exhibits two interfaces when $H \neq 0$, the first interface being that between the air and the oil, and the second interface being that between the oil layer and the water. When $H = 0$, the target liquid exhibits only the first interface between air and water. We neglect the deformation of the impinging droplet when there is no oil layer, since the surface area of the deformed droplet is much smaller than the surface area of the crater. When $H = 0$ or $H > d$, only the first interface is deformed. In this case, the change in the surface energy is obtained by subtracting the original surface area before the impact, πd^2, from the area of the hemispherical crater, $2\pi d^2$. Therefore, the change in the surface energy is simply $\Delta E_s = \sigma\,\pi d^2$, where σ is the surface tension of the first interface: either the surface tension between water and air σ_{wa} or that between oil and air σ_{oa}. Second, when $0 < H < d$, both the first and the second interfaces are deformed. In this model, we assume that the first interface is deformed to become hemispherical and that the second interface is deformed to follow the first interface where $-d < z < -H$. The extra surface area of the second interface is obtained by subtracting the smaller plane circle, $\pi(d^2 - H^2)$, from the area of the hemispherical cap, $\int_0^{2\pi} \mathrm{d}\phi \int_0^{\theta'} d^2 \sin\theta\ \mathrm{d}\theta = 2\pi(d^2 - dH)$, where $\theta' = \cos^{-1}(H/d)$.

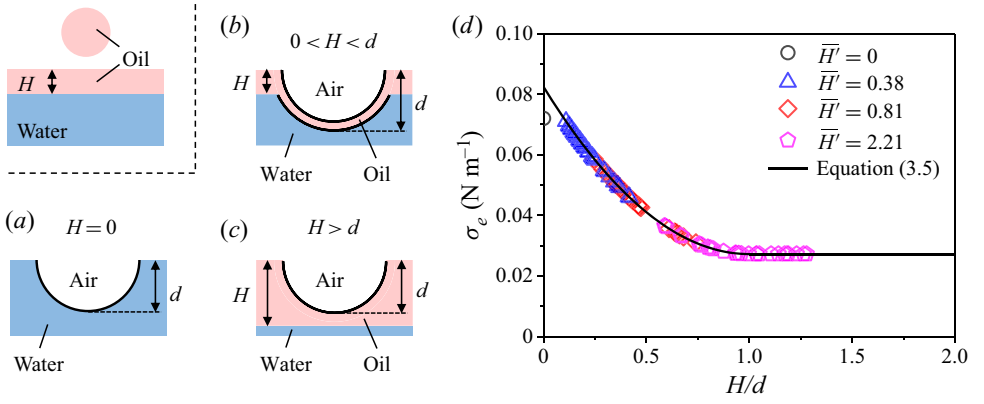

FIGURE 5. A dual-interface model, showing oil–air interface (red) and oil–water interface (blue). (*a*) When no oil layer exists, the surface area to be considered is the sum of the area of the crater. The surface area of the deformed impinging droplet is neglected. (*b*) When the thickness of the oil layer is comparable to the size of the crater, the deformation of the second interface between the oil and the water needs to be considered. (*c*) When the oil layer is thick enough, the second interface does not contribute to the energetic analysis. (*d*) The calculation of (3.5) using $\sigma_{wa} = 72$ mN m^{-1}, $\sigma_{ow} = 55.2$ mN m^{-1} and $\sigma_{oa} = 27.2$ mN m^{-1}. The solid line is (3.5). We note that the model is continuous except at $H/d = 0$.

Summing up, the change in the surface energy is expressed using an effective surface tension σ_e such that $\Delta E_s = \sigma_e \pi d^2$, where

$$\sigma_e = \begin{cases} \sigma_{wa} & \text{for } H = 0, \\ \sigma_{oa} + \sigma_{ow}(1 - H/d)^2 & \text{for } 0 < H < d, \\ \sigma_{oa} & \text{for } H > d. \end{cases} \tag{3.5}$$

Using the surface tension values $\sigma_{wa} = 72$ mN m^{-1}, $\sigma_{ow} = 55.2$ mN m^{-1} and $\sigma_{oa} = 27.2$ mN m^{-1} (Goebel & Lunkenheimer 1999), we present the calculation of (3.5) in figure 5(*d*). This shows that σ_e is smallest when H is relatively large and that it is greatest ($\sigma_e \simeq \sigma_{oa} + \sigma_{ow} > \sigma_{wa}$) when H is small but non-zero.

Finally, we postulate that all the kinetic energy of the impinging droplet is transferred to gravitational potential energy and additional surface energy, that is,

$$E_k = E_p + \Delta E_s. \tag{3.6}$$

Using (3.1), (3.4) and (3.5), equation (3.6) becomes a quartic equation of d' in terms of Fr,

$$\left.\begin{array}{ll} (1+\rho')d'^4 + 4\sigma'_{wa}d'^2 - Fr/3 = 0 & \text{for } H' = 0, \\ (1+\rho')d'^4 + (4\sigma'_{oa} + 4\sigma'_{ow} - 2\rho' H'^2)d'^2 & \\ \quad - 8\sigma'_{ow}H'd' + (4\sigma'_{ow}H'^2 - Fr/3 + \rho' H'^4) = 0 & \text{for } 0 < H' < d', \\ d'^4 + 4\sigma'_{oa}d'^2 - Fr/3 = 0 & \text{for } H' > d', \end{array}\right\} \tag{3.7}$$

where $\sigma' = \sigma/(\rho_o g D^2)$ and $\rho' = \rho_w/\rho_o - 1$.

We solve for the roots of the quartic equation in (3.7), and each root is shown in figure 4(*b*). For each run of the experiment, we calculated the positive root d'_e of (3.7)

using the inputs U, D and H from experiments. Physically, d'_e is the maximum depth of the cavity, as expected when the deformation of the second interface is considered. When $Fr > 100$, it can be seen that d'_e follows the classical scaling relation in (1.1). Otherwise, d'_e deviates significantly from the one-fourth power law. For example, when Fr is relatively small, d'_e in fact decreases as Fr increases. In this regime, the surface deformation takes a relatively larger portion of the energy than the gravitational potential energy, namely $\Delta E_s > E_p$, and the one-fourth power law, which was derived using $E_k = E_p$, does not apply. In the limit of $\Delta E_s \gg E_p$, the energy balance between E_k and ΔE_s is simply written as $D^3U^2 \sim \sigma d^2$, from which a different scaling relation $d' \sim We^{1/2}$ is inferred. For a fixed U, the increase of D increases We but decreases Fr, so we observe the inverse scaling between d' and Fr in figure 4(*b*). This feature is also observed in experiments, as shown in figure 4(*a*). The agreement between the simple model and the data suggests that the model accounts correctly for the underlying physics.

3.3. *The height of the jet and the pinch-off modes*

In figure 6(*a*), we present measurements of the maximum height of the Worthington jet $\ell' = \ell/D$ with respect to the effective Weber number, which we define as $We_e = \rho_o U^2 D/\sigma_e$ using the effective surface tension σ_e in (3.5). We note that the error bars are large for the case of $H' = 0$, because premature pinch-off of child droplets causes uncertainty in the estimation of ℓ.

We find that ℓ' increases with We_e, following the power law $\ell' \sim We_e^{\alpha}$, where $\alpha = 1.0 \pm 0.2$ is calculated from linear fitting after transforming ℓ' and We_e into a logarithmic scale. It is generally reported that $\ell' \sim We$ in the literature (Ray, Biswas & Sharma 2012; Ray *et al.* 2015; Che & Matar 2018), but the scaling relation does not apply to our case because the conventional definition of the Weber number is independent of H'. To address this problem, we use the effective Weber number from σ_e, and thus We_e also depends on H'. Our measurement of ℓ' then collapses into a similar scaling relation $\ell' \sim We_e$, as shown in figure 6(*a*). This result suggests that the model in (3.5) correctly estimates the surface energy with the presence of the oil layer and that the overall dynamical features of the impingement are well captured by the dual-interface model presented in figure 5.

Figure 6(*b*) shows a map of the pinch-off modes using individual measurements of ℓ', since the average value ℓ' of the repeated measurements includes the different pinch-off modes when a large deviation occurs. We identify two pinch-off modes depending on the location of the detachment of child droplets. When a child droplet is detached in the upper part of the jet, the mode is termed 'upper pinch-off'. In the opposite case, the mode is termed 'lower pinch-off' (Kim *et al.* 2018). The sequential images show examples of the pinch-off modes during impingement (figure 6*c*,*d*). As a general trend, upper pinch-off modes are observed when the effective Weber number is relatively large or the oil layer is thicker. Lower pinch-off modes are observed when the oil layer is thinner or absent. Both modes are observed only when the jet reaches above a critical height, namely $\ell' > 2$. We speculate that the existence of the critical height can be explained by the Plateau–Rayleigh instability. Empirically, the diameter $2R_0$ of the jet approximately equals the droplet diameter, namely $2R_0 \simeq D$. This renders the fastest-growing wavelength of the Plateau–Rayleigh instability to be $\lambda_m = 9R_0$, and $\ell > \lambda_m/2$ is required to have a local minimum of the undulation (Rayleigh 1878). This simple theoretical consideration yields $\ell' > 2.25$ as the criterion for pinch-off. The location of the pinch-off is then determined by the inertia of the jet and the surface tension: the upper pinch-off tends to occur at higher

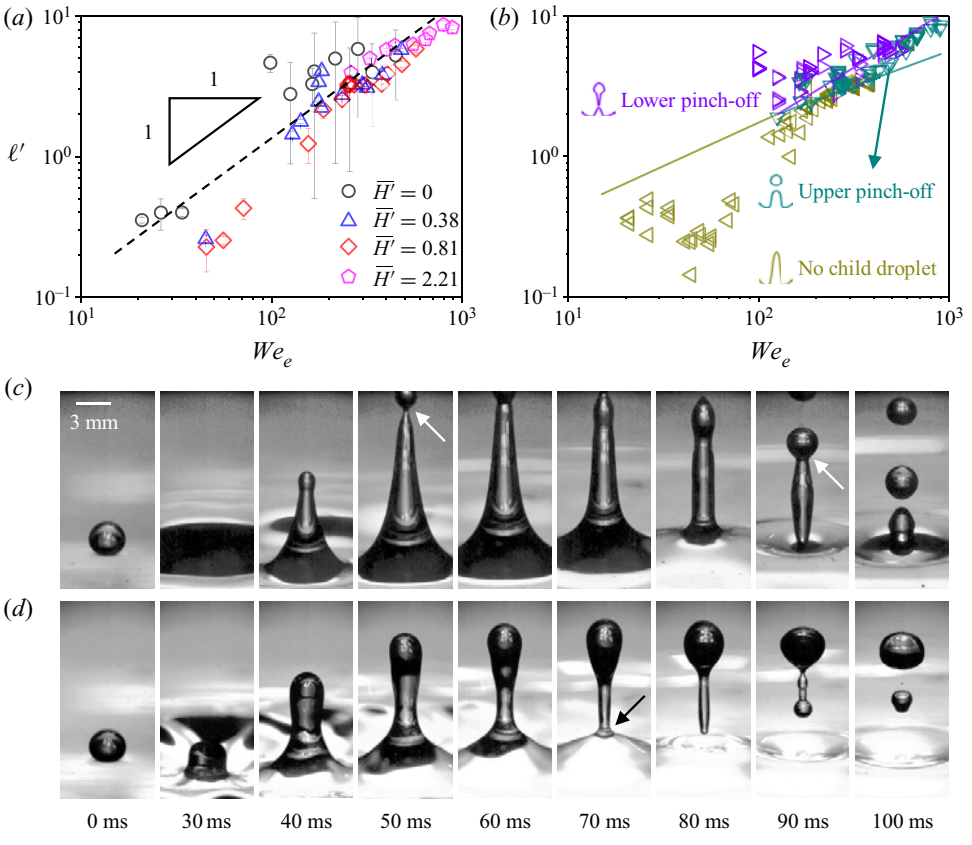

FIGURE 6. Jet height and the pinch-off of child droplets. (*a*) The dimensionless maximum height of the jet, ℓ', with respect to the effective Weber number $We_e \equiv \rho U^2 D/\sigma_e$ for $\overline{H'} = 0$, 0.38, 0.81 and 2.21. The dashed line is drawn to clarify the slope of 1. (*b*) The individual observations of the pinch-off position: no child droplet (◁), upper pinch-off (▽) and lower pinch-off (▷). (*c*, *d*) Example images of pinch-off modes for case C2: (*c*) $H' = 1.60$ (upper pinch-off) and (*d*) $H' = 0.33$ (lower pinch-off). The arrows indicate the position of the pinch-off.

Weber number, where the inertial force wins over the surface tension. This picture of the pinch-off is consistent with the work by Kim *et al.* (2018).

4. Conclusion

In conclusion, we investigated the phenomena occurring when an oil droplet impinges onto an oil-layered water bath. In the experiment, we varied the diameter and impact velocity of the droplet and the thickness of the oil layer to characterize the impingement dynamics for a two-layer liquid. As with similar studies using a single-layer liquid, a crater is formed at the point of impact, and the ejection of a Worthington jet follows. By using high-speed video imaging, we measured the depth of the crater d' and the height of the jet ℓ', normalized by the droplet diameter D. Our measurements suggest that, even though the overall dynamics of the impingement are similar to the single-layer case, the detailed measurements vary with the thickness of the oil layer $H' \equiv H/D$. Both d' and ℓ' are smaller when a thin oil layer ($0 < H' < \sim 1.60$) is present than when no oil layer is present.

Interestingly, when the thickness of the oil layer further increases ($H' > \sim 1.60$), both quantities also increase. This observation indicates that the qualitative features of a thick oil layer are similar those of an oil layer of zero thickness.

To rationalize our observation, we established a mathematical model that added a second interface to the classical model for droplet impingement. In the model, we balance the kinetic energy of the impinging droplet with the gravitational potential energy of the displaced liquid and the excess surface energy of the crater. The crater is assumed to be hemispherical, and the gravitational potential energy and the surface energy are integrated using the density and the interfacial tension of each layer. The value of d' can then be estimated using the model with experimental parameters as inputs, and a rough agreement with the classical scaling relation with the Froude number was observed. Furthermore, based on the model, we also defined an effective surface tension σ_e and a corresponding effective Weber number We_e because the conventional Weber number is unable to represent the impingement results with respect to H'. We found that our measurement of ℓ' collapsed into a single scaling relation only when We_e was used. These observations suggest that our model captures the dynamics well. This work could be applied to fundamental and industrial problems involving droplets impinging onto a two-layer liquid, such as the spraying of oil dispersants.

Acknowledgements

This study was supported by the National Research Foundation of Korea (NRF) grant funded by the Korean government (MSIT) (No. 2020R1A2C3010568) and the New and Renewable Energy Core Technology Program of the Korea Institute of Energy Technology Evaluation and Planning (KETEP) with a grant of financial resources from the Ministry of Trade, Industry and Energy, Republic of Korea (No. 20193010014740).

Declaration of interests

The authors report no conflict of interest.

REFERENCES

BISIGHINI, A., COSSALI, G. E., TROPEA, C. & ROISMAN, I. V. 2010 Crater evolution after the impact of a drop onto a semi-infinite liquid target. *Phys. Rev.* E **82** (3), 036319.

BOREYKO, J. B., POLIZOS, G., DATSKOS, P. G., SARLES, S. A. & COLLIER, C. P. 2014 Air-stable droplet interface bilayers on oil-infused surfaces. *Proc. Natl Acad. Sci. USA* **111** (21), 7588–7593.

CASTILLO-OROZCO, E., DAVANLOU, A., CHOUDHURY, P. K. & KUMAR, R. 2015 Droplet impact on deep liquid pools: Rayleigh jet to formation of secondary droplets. *Phys. Rev.* E **92** (5), 053022.

CHE, Z. & MATAR, O. K. 2018 Impact of droplets on immiscible liquid films. *Soft Matt.* **14** (9), 1540–1551.

COSSALI, G. E., MARENGO, M., COGHE, A. & ZHDANOV, S. 2004 The role of time in single drop splash on thin film. *Exp. Fluids* **36** (6), 888–900.

ENGEL, O. G. 1965 Crater depth in fluid impacts. *J. Appl. Phys.* **37**, 1798–1808.

FEDORCHENKO, A. I. & WANG, A.-B. 2004 On some common features of drop impact on liquid surfaces. *Phys. Fluids* **16** (5), 1349–1365.

FINGAS, M. 2012 *The Basics of Oil Spill Cleanup*. CRC Press.

FUJIMATSU, T., FUJITA, H., HIROTA, M. & OKADA, O. 2003 Interfacial deformation between an impacting water drop and a silicone-oil surface. *J. Colloid Interface Sci.* **264** (1), 212–220.

GHABACHE, É., SÉON, T. & ANTKOWIAK, A. 2014 Liquid jet eruption from hollow relaxation. *J. Fluid Mech.* **761**, 206–219.

GOEBEL, A. & LUNKENHEIMER, K. 1999 Interfacial tension of the water/n-alkane interface. *Langmuir* **13**, 369–372.

JAIN, U., JALAAL, M., LOHSE, D. & VAN DER MEER, D. 2019 Deep pool water-impacts of viscous oil droplets. *Soft Matt.* **15**, 4629–4638.

KIM, S. J., KIM, S. & JUNG, S. 2018 Extremes of the pinch-off location and time in a liquid column by an accelerating solid sphere. *Phys. Rev. Fluids* **3** (8), 084001.

LENG, L. J. 2001 Splash formation by spherical drops. *J. Fluid Mech.* **427**, 73–105.

LESSARD, R. R. & DEMARCO, G. 2000 The significance of oil spill dispersants. *Spill Sci. Technol. Bull.* **6** (1), 59–68.

MACKLIN, W. C. & METAXAS, G. J. 1976 Splashing of drops on liquid layers. *J. Appl. Phys.* **47** (9), 3963–3970.

MANZELLO, S. L. & YANG, J. C. 2002 An experimental study of a water droplet impinging on a liquid surface. *Exp. Fluids* **32** (5), 580–589.

MICHON, G.-J., JOSSERAND, C. & SÉON, T. 2017 Jet dynamics post drop impact on a deep pool. *Phys. Rev. Fluids* **2**, 023601.

MURPHY, D. W., LI, C., D'ALBIGNAC, V., MORRA, D. & KATZ, J. 2015 Splash behaviour and oily marine aerosol production by raindrops impacting oil slicks. *J. Fluid Mech.* **780**, 536–577.

PROSPERETTI, A. & OGUZ, H. N. 1993 The impact of drops on liquid surfaces and the underwater noise of rain. *Annu. Rev. Fluid Mech.* **25** (1), 577–602.

PUMPHREY, H. C. & ELMORE, P. A. 1990 The entrainment of bubbles by drop impacts. *J. Fluid Mech.* **220**, 539–567.

RAY, B., BISWAS, G. & SHARMA, A. 2012 Bubble pinch-off and scaling during liquid drop impact on liquid pool. *Phys. Fluids* **24** (8), 082108.

RAY, B., BISWAS, G. & SHARMA, A. 2015 Regimes during liquid drop impact on a liquid pool. *J. Fluid Mech.* **768**, 492–523.

RAYLEIGH, LORD 1878 On the instability of jets. *Proc. Lond. Math. Soc.* **1** (1), 4–13.

SHAIKH, S., TOYOFUKU, G., HOANG, R. & MARSTON, J. O. 2018 Immiscible impact dynamics of droplets onto millimetric films. *Exp. Fluids* **59** (1), 7.

SMOLKA, L. B. & MCLAUGHLIN, C. K. 2019 Sphere entry through an oil lens floating on water. *Phys. Rev. Fluids* **4** (4), 044001.

WANG, A.-B. & CHEN, C.-C. 2000 Splashing impact of a single drop onto very thin liquid films. *Phys. Fluids* **12** (9), 2155–2158.

WANG, W., JI, C., LIN, F., WEI, X. & ZOU, J. 2019 Formation of water in oil in water particles by drop impact on an oil layer. *Phys. Fluids* **31** (3), 037107.

WORTHINGTON, A. M. 1908 *A Study of Splashes*. Longmans, Green, and Company.

XU, M., WANG, C. & LU, S. 2017 Water droplet impacting on burning or unburned liquid pool. *Exp. Therm. Fluid Sci.* **85**, 313–321.

YILMAZ, N. & NELSON, R. 2014 Cavity dynamics of smooth sphere and golf ball at low froude number, part 1: high-speed imaging and quantitative measurements. *J. Vis. Japan* **18** (2), 335–342.